Electronic Supplementary Material (ESI) for Inorganic Chemistry Frontiers.

Electronic Supplementary Information

Fabrication of high-surface-area mesoporous frameworks of β-$Ni(OH)_2$-$CdIn_2S_4$ p-n nano-heterojunctions for improved visible light photocatalytic hydrogen production

Evangelos K. Andreou, Ioannis Vamvasakis and Gerasimos S. Armatas*
Department of Materials Science and Engineering, University of Crete, Heraklion 70013, Greece

*E-mail: garmatas@materials.uoc.gr

Supporting Tables

Table S1. Elemental composition of mesoporous CIS and Ni-modified CIS NCFs, and 10% Ni-modified CIS microparticles.

Sample	Cd (at%)	In (at%)	S (at%)	Ni (at%)	Ni loading[a)] (wt%)
CIS NCFs	15.50	29.90	54.60	-	-
5-Ni/CIS NCFs	15.13	27.30	50.63	6.94	5.40
7-Ni/CIS NCFs	14.12	28.10	48.98	8.80	7.22
10-Ni/CIS NCFs	13.00	26.74	48.65	11.61	10.02
15-Ni/CIS NCFs	12.67	24.86	44.40	18.07	15.11
10-Ni/CIS-*m*	13.07	26.68	48.33	11.92	10.20

[a)] Based on the EDS Ni to Cd atomic ratio.

Table S2. Photocatalytic efficiency comparison of several thiospinel-based photocatalysts.

Photocatalyst	Reaction Conditions	Light Source	H_2 evolution rate		Quantum Efficiency (QE)	Ref.
			($\mu mol\ h^{-1}$)	($\mu mol\ g^{-1}\ h^{-1}$)		
3 wt.% Pt/5 wt.% Co_9S_8/ $CdIn_2S_4$	50 mg catalyst, 20% v/v TEOA	300 W Xe lamp ($\lambda \geq 420$ nm)	54	1083.6	5.5% at 420 nm	1
$CdIn_2S_4$@CoAl-LDH	2 mg catalyst, 10% v/v TEOA	300 W Xe lamp ($\lambda \geq 420$ nm)	1.6	793.4	0.2% at 450 nm	2
$CdIn_2S_4/In(OH)_3/Zn_2GeO_4$	50 mg catalyst, 0.35 M Na_2S, 0.25 M Na_2SO_3	300 W Xe lamp ($\lambda \geq 420$ nm)	71	1426.90	9.1% at 420 nm	3
1 wt.% MoS_2/ $CdIn_2S_4$	50 mg catalyst, 0.35 M Na_2S, 0.25 M Na_2SO_3	300 W Xe lamp ($\lambda \geq 420$ nm)	47.3	2365	5.2% at 400 nm	4
$CdIn_2S_4/In(OH)_3$/NiCr-LDH	50 mg catalyst, 0.35 M Na_2S, 0.25 M Na_2SO_3	300 W Xe lamp ($\lambda \geq 420$ nm)	54.65	1093	1.7% at 420 nm	5
$CdIn_2S_4$/rGO/ZnS QDs	50 mg catalyst, 6% v/v TEOA	300 W Xe lamp ($\lambda \geq 420$ nm)	341	6820	19.3% at 430 nm	6
$CdIn_2S_4/CNFs/Co_4S_3$	50 mg catalyst, 20% v/v lactic acid	300 W Xe lamp ($\lambda \geq 420$ nm)	1293.5	25870	16.3% at 420 nm	7
$CdIn_2S_4$/ZnS	20 mg catalyst, 0.35 M Na_2S, 0.25 M Na_2SO_3	300 W Xe lamp	74.8	3743	2.2% at 365 nm	8
$CdIn_2S_4/ZnIn_2S_4$	4 mg catalyst, 0.35 M Na_2S, 0.25 M Na_2SO_3	300 W Xe lamp ($\lambda \geq 420$ nm)	50.7	12670	18.7% at 420 nm	9
Co-Pi/$CdIn_2S_4$	10 mg catalyst, 20% v/v MeOH	500 W Xe lamp ($\lambda \geq 420$ nm)	72.8	7280	14.1% at 405 nm	10
$Ni_{12}P_5/CdIn_2S_4$	30 mg catalyst, 10% v/v TEOA	300 W Xe lamp ($\lambda \geq 420$ nm)	150.3	5010	23.5% at 400 nm	11
$Ni_2P/ZnIn_2S_4$	50 mg catalyst, 10% v/v lactic acid	300 W Xe lamp ($\lambda > 400$ nm)	103.3	2066	7.7% at 420 nm	12
$CoP/ZnIn_2S_4$	20 mg catalyst, 0.35 M Na_2S, 0.25 M Na_2SO_3	300 W Xe lamp ($\lambda \geq 420$ nm)	175.5	8775	24.1% at 420 nm	13
$Pt/Cu_3P/ZnIn_2S_4$	50 mg catalyst, 0.35 M Na_2S,	300 W Xe lamp ($\lambda \geq 420$ nm)	128	2561	22.3% at 420 nm	14

	0.25 M Na_2SO_3					
$Ni_{12}P_5/ZnIn_2S_4$	50 mg catalyst, 0.35 M Na_2S, 0.25 M Na_2SO_3	300 W Xe lamp (λ≥420 nm)	113	2263	20.5% at 420 nm	15
$CoP@ZnIn_2S_4$	10 mg catalyst, 10% v/v TEOA	300 W Xe lamp (λ≥420 nm	103	10300	16.2% at 420 nm	16
15 wt.% $Ni_2P/CdIn_2S_4$	20 mg catalyst, 10% v/v TEOA	300 W Xe lamp (λ≥420 nm)	586	29300	61.7% at 420 nm	17
10 wt.% *β*-$Ni(OH)_2$/ $CdIn_2S_4$	**20 mg catalyst, 10% v/v TEOA**	**300 W Xe lamp (λ≥420 nm)**	**395**	**19750**	**52.0 % at 420 nm**	**This work**

Table S3. Nyquist equivalent circuit fitted parameters of the prepared materials.

Sample	**R_s (Ω)**	**C_{dl} (F)**	**R_{ct} (Ω)**	**x^2**
CIS NCFs	12.46	46×10^{-6}	565	3.60×10^{-3}
5-Ni/CIS NCFs	14.72	185×10^{-6}	346	1.95×10^{-4}
7-Ni/CIS NCFs	13.51	195×10^{-6}	265	3.06×10^{-3}
10-Ni/CIS NCFs	12.19	144×10^{-6}	238	4.16×10^{-3}
15-Ni/CIS NCFs	12.70	221×10^{-6}	373	2.16×10^{-3}
10-Ni/CIS-*m*	13.79	58×10^{-6}	1104	3.53×10^{-3}
β-$Ni(OH)_2$	13.36	39×10^{-6}	3437	3.13×10^{-3}

Supporting Figures

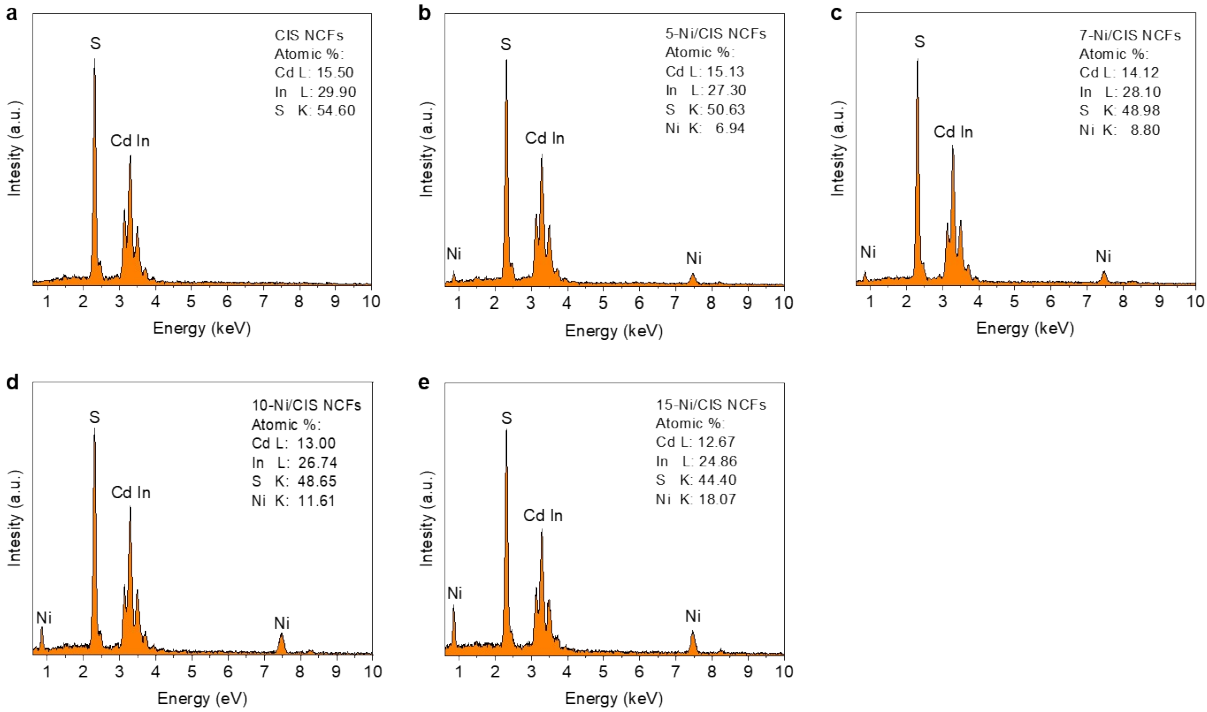

Fig. S1 Typical EDS spectra of the mesoporous CIS and Ni-modified CIS NCFs materials.

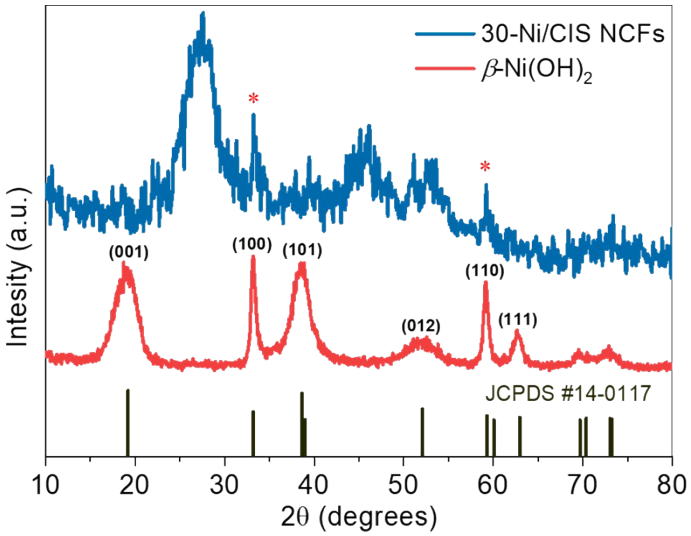

Fig. S2 XRD patterns of the as-prepared 30 wt.% Ni-loaded CIS (30-Ni/CIS NCFs) and isolated β-$Ni(OH)_2$ microparticles. The diffraction peaks at 2θ = 33° and 59° scattering angles (marked with symbol *) in the XDR pattern of 30-Ni/CIS NCFs can be attributed to the (100) and (110) reflections of the hexagonal β-$Ni(OH)_2$ structure. The XRD pattern of the as-prepared β-$Ni(OH)_2$ microparticles is consistent with the standard diffraction pattern of hexagonal β-$Ni(OH)_2$ (JCPDS card no. 14-0117).

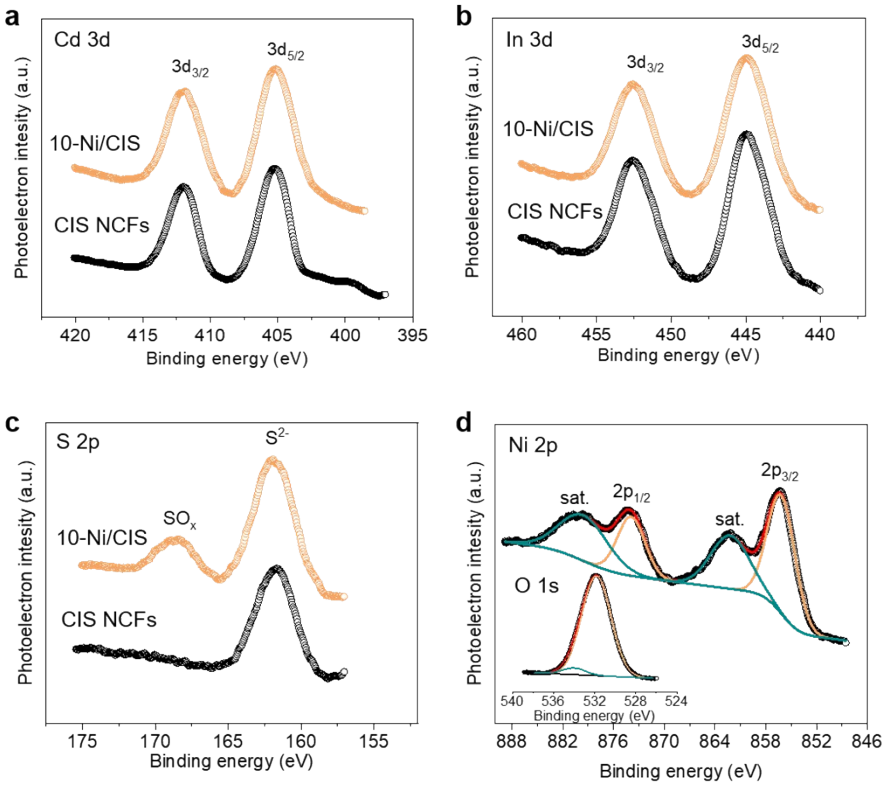

Fig. S3 Typical XPS core-level spectra of the (a) Cd 3d, (b) In 3d, (c) S 2p, and (b) Ni 2p and O 1s (inset) regions of mesoporous CIS and 10-Ni/CIS NCFs catalysts.

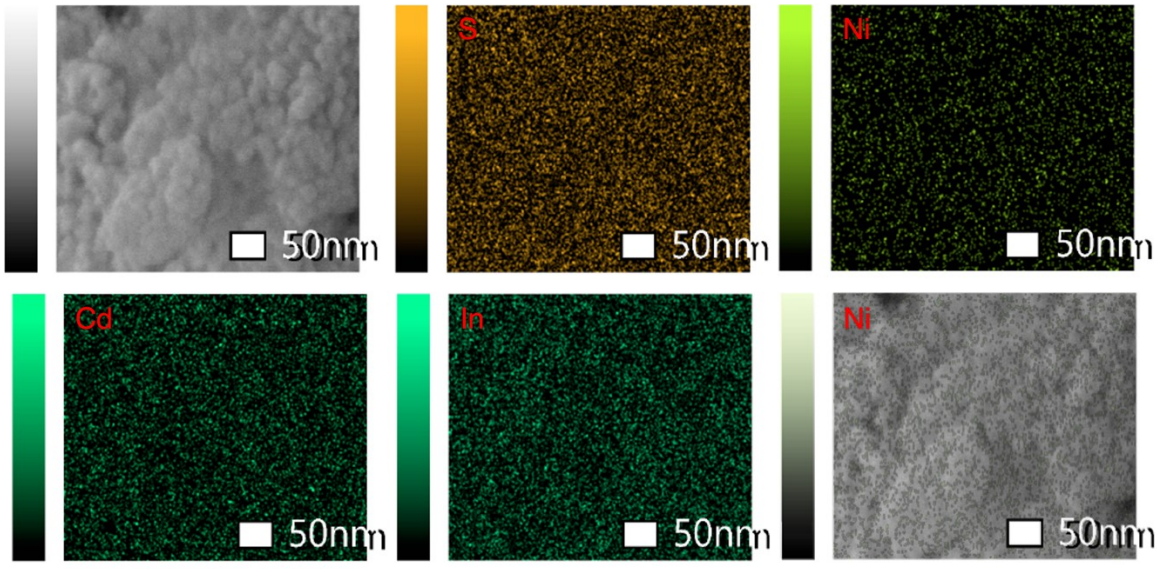

Fig. S4 EDS elemental mapping of 10-Ni/CIS NCFs catalyst. The homogeneous distribution of Ni atoms (green spots in the lower-right panel) on the surface of the catalyst is also depicted.

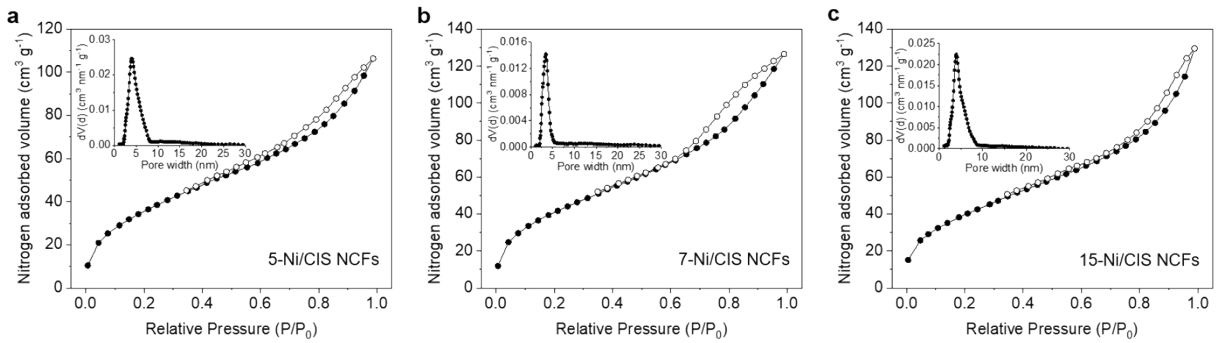

Fig. S5 Nitrogen adsorption (filled cycles) and desorption (open cycles) isotherms at –196 °C for the Ni-modified CIS samples with 5, 7 and 15 wt.% Ni content. Insets: The corresponding NLDFT pore-size distribution plots derived from the adsorption isotherms.

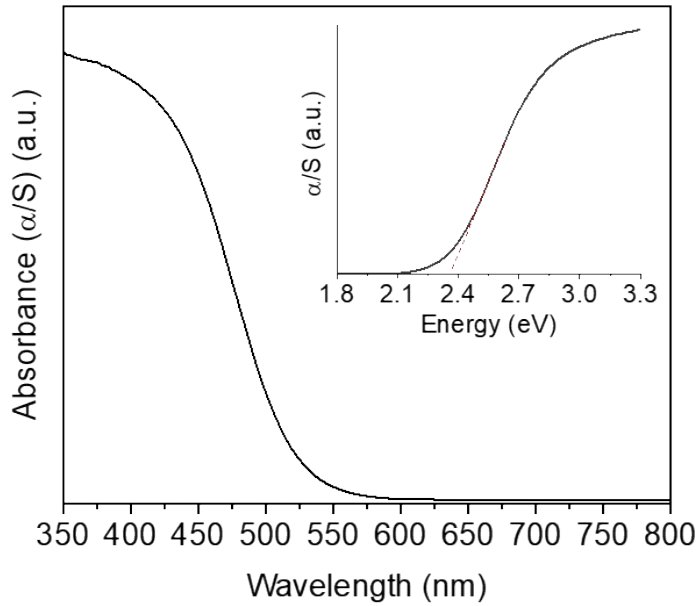

Fig. S6 UV-vis spectrum of bulk CIS. Inset: the corresponding Kubelka-Munk plot showing an energy bandgap of 2.36 eV.

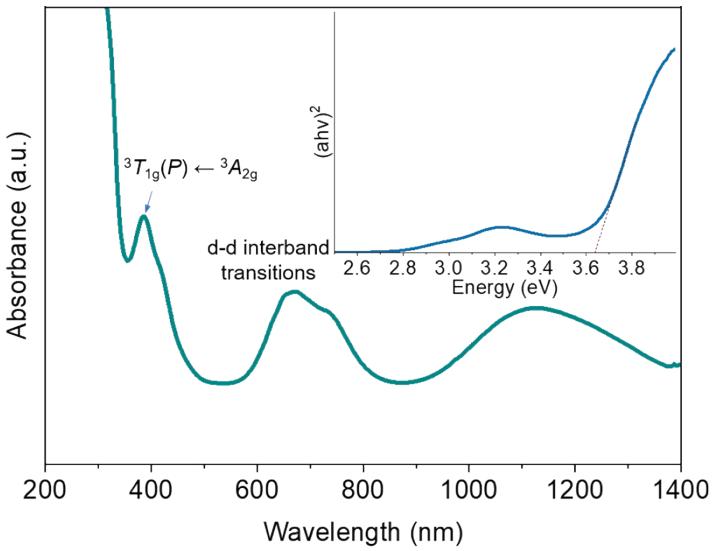

Fig. S7 UV-vis/NIR spectrum of the as-prepared β-Ni(OH)$_2$ microparticles, showing the characteristic d-d interband transitions at ~385, ~670 and ~1120 nm. The steep absorption bellow 350 nm corresponding to the band-gap transition. Inset: the corresponding Tauc plot for direct band gap semiconductor, showing an energy bandgap of ~3.65 eV.

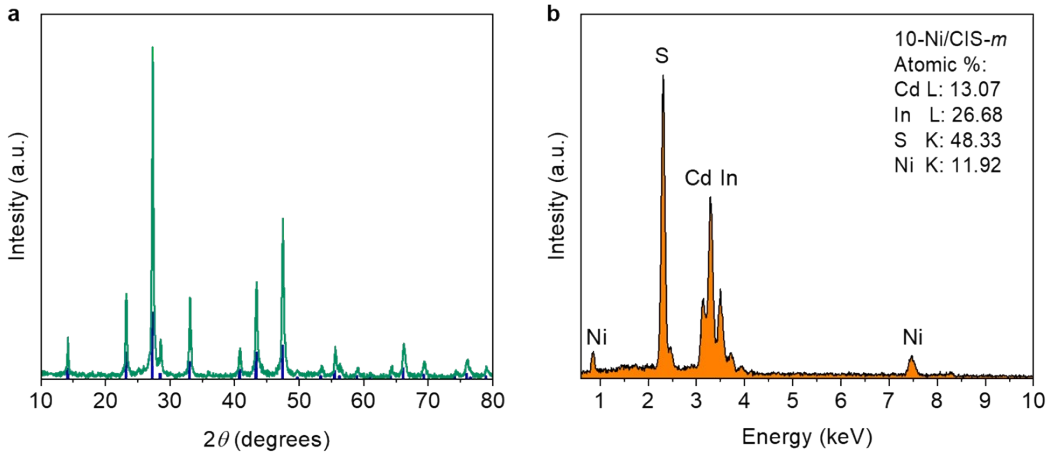

Fig. S8 Typical (a) XRD pattern and (b) EDS spectrum of bulk 10-Ni/CIS-*m*. In panel (a), the blue lines correspond to the standard diffraction of cubic $CdIn_2S_4$ (space group: Fd3m), according to JCPDS card no. 27-0060. The EDS data give a Ni content of 10.2 wt.%.

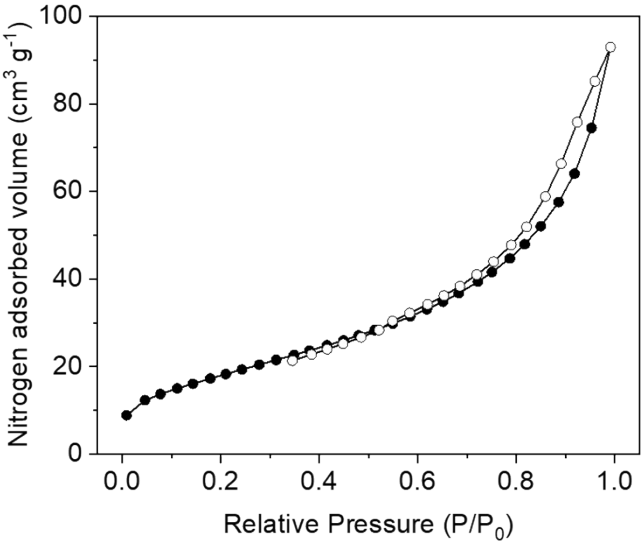

Fig. S9 Nitrogen adsorption (filled cycles) and desorption (open cycles) isotherms at –196 °C for the bulk 10-Ni/CIS-*m* reference material.

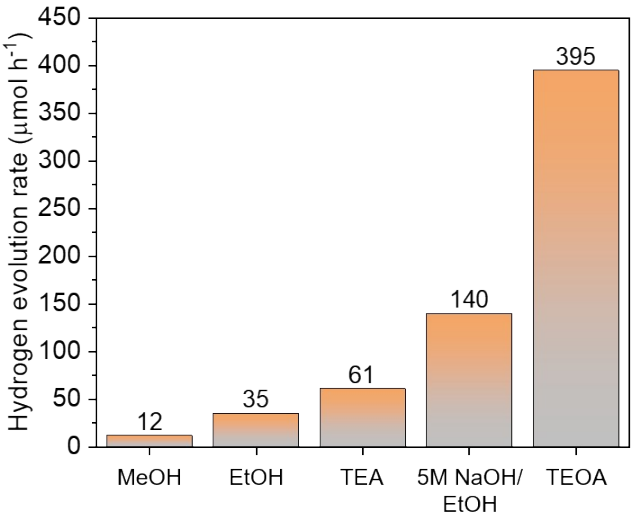

Fig. S10 Hydrogen evolution activity of the 10-Ni-CIS NCFs photocatalyst, using different sacrificial reagents: methanol (MeOH, 10% v/v), ethanol (EtOH, 10% v/v), triethylamine (TEA, 10% v/v), 5M NaOH/Ethanol (EtOH, 10% v/v) and triethanolamine (TEOA, 10% v/v). Reaction conditions: 20 mg of photocatalyst was dispersed in a 20 mL aqueous solution containing the respective hole scavenger, 300-W Xe-lamp equipped with a UV-cut off filter ($\lambda \geq 420$ nm).

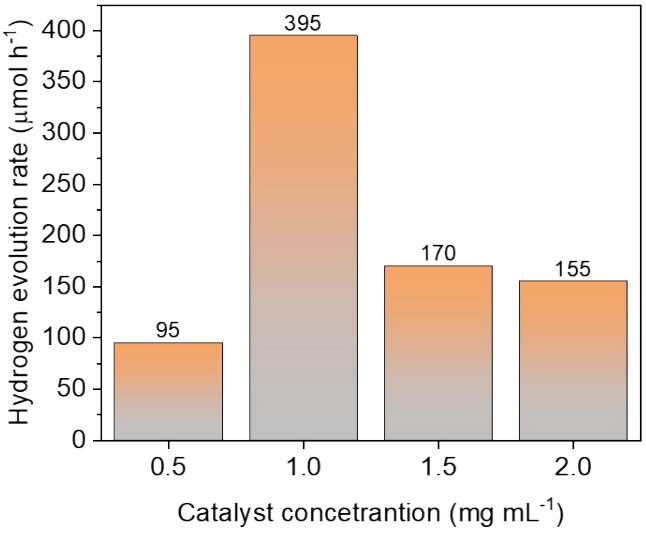

Fig. S11 Hydrogen evolution activity of 10-Ni-CIS NCFs photocatalysts, using different catalyst loading. Reaction conditions: 10-40 mg of catalyst was dispersed in a 20 mL aqueous solution of TEOA (10% v/v), 300-W Xe-lamp equipped with a UV-cut off filter (λ ≥420 nm).

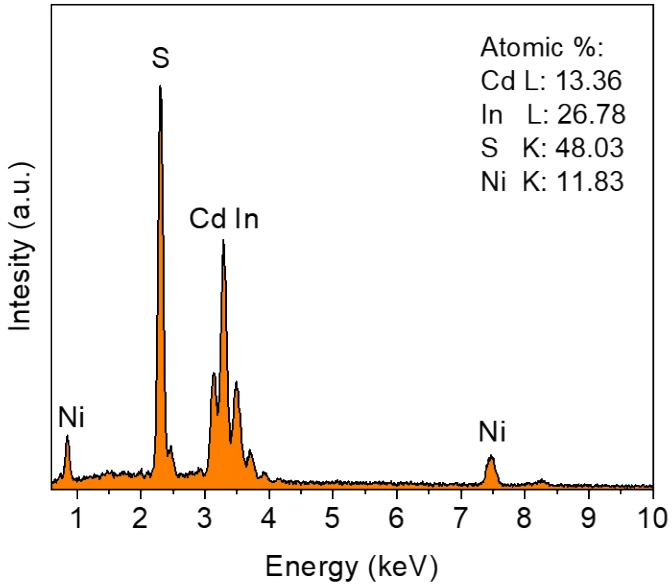

Fig. S12 Typical EDS spectrum of the reused 10-Ni/CIS NCFs catalyst. The EDS analysis gives a 9.95 wt.% Ni content.

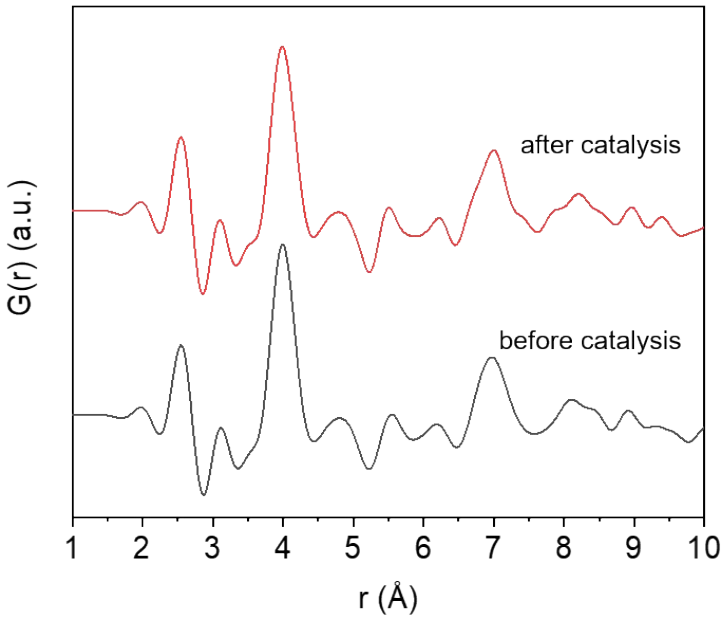

Fig. S13 Reduced atomic pair distribution function G(r) plots of the 10-Ni/CIS NCFs before and after photocatalysis. The reused 10-Ni/CIS NCFs catalyst exhibits a PDF profile nearly identical to that of the fresh sample, indicating a similar atomic structure.

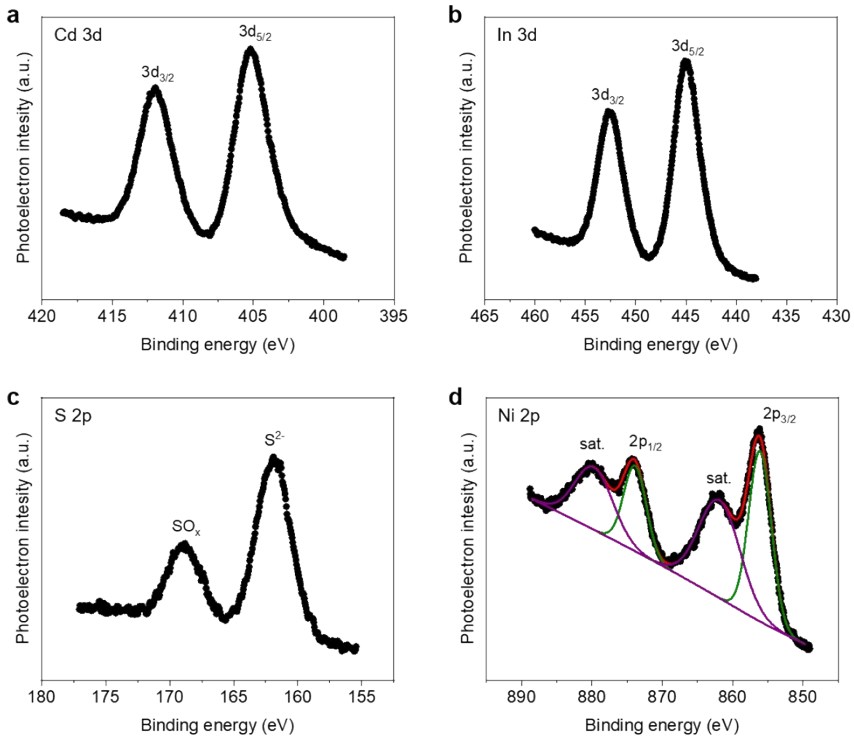

Fig. S14 Typical XPS spectra of a) Cd 3d, b) In 3d, c) S 2p and d) Ni 2p of the 10-Ni/CIS NFAs photocatalyst after four-five hours catalytic runs.

The Cd 3d XPS spectrum of the reused photocatalyst (10-Ni/CIS NCFs) shows a doublet peak at 405.1 and 411.9 eV, corresponding to the Cd $3d_{5/2}$ and Cd $3d_{3/2}$ spin-orbits of Cd^{2+}, respectively. Meanwhile, the In 3d XPS spectrum reveals photoelectron signals attributed to the In $3d_{5/2}$ (445.0 eV) and In $3d_{3/2}$ (452.5 eV) spin-orbit components of In^{3+} cations in $CdIn_2S_4$. In the S 2p XPS spectrum, the signal at 161.9 eV corresponds to the S^{2-} valence state, whereas the broad peak at 168.8 eV arises from surface

SO_x species. In the Ni 2p XPS region, two prominent peaks of Ni $2p_{3/2}$ and Ni $2p_{1/2}$ are observed at 856.1 and 873.9 eV, respectively, attributed to Ni^{2+} cations in $Ni(OH)_2$. Additionally, the presence of strong satellite signals at 861.9 and 879.7 eV further confirms the paramagnetic nature of Ni(II).

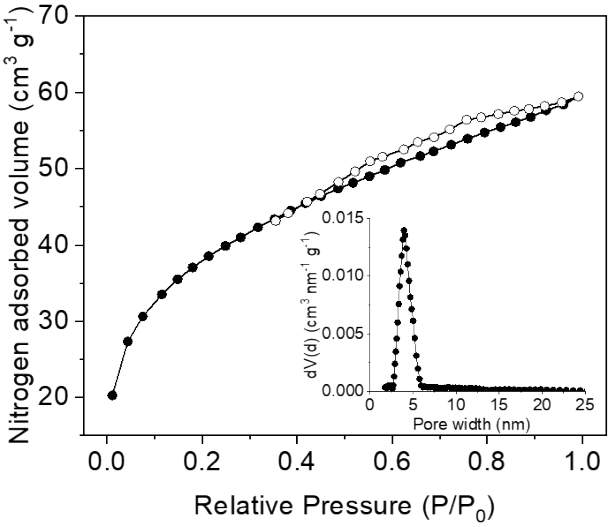

Fig. S15 N_2 adsorption and desorption isotherms at –196 °C of the 10-Ni/CIS NCFs catalyst after 20 h photocatalytic test. Analysis of the adsorption data gives a surface area of 133 m^2 g^{-1}, a total pore volume of 0.1 cm^3 g^{-1} and an average pore width of 4.0 nm.

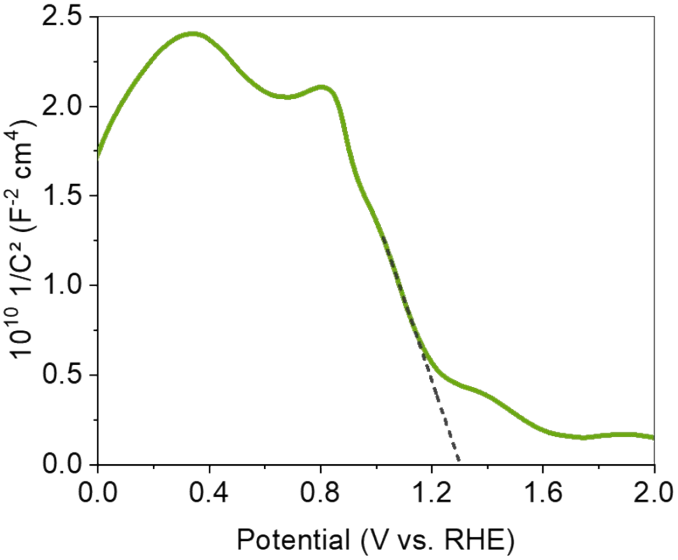

Fig. S16 Mott-Schottky plot for the as-prepared β-$Ni(OH)_2$ microparticles. The linear fit to the data (dashed line) gives a E_{FB} of ~1.30 V (vs RHE) at pH 7, while the positive slope indicates p-type conductivity. Given an energy bandgap of 3.65 eV, the conduction band energy (E_C) of β-$Ni(OH)_2$ was calculated as –2.35 V (vs RHE) at pH 7.

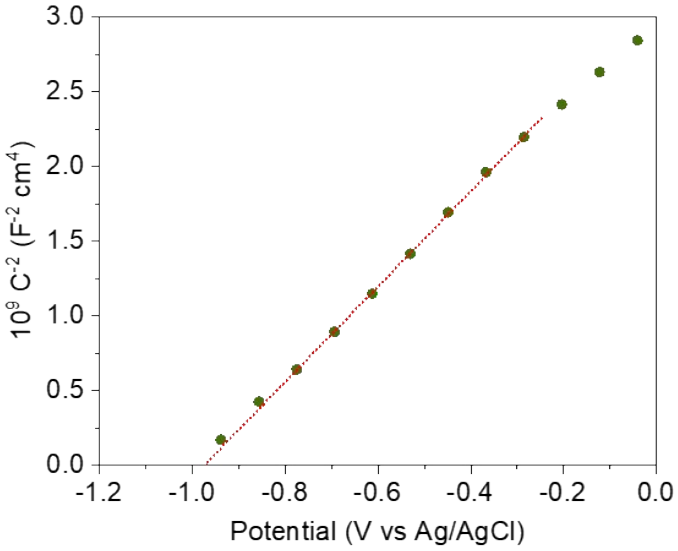

Fig. S17 Mott-Schottky plot for the bulk CIS. The linear fit to the date (red dashed line) gives a E_{FB} of –0.77 V (vs RHE) at pH 7 and a donor concentration (N_D) of ~6.6×10^{17} cm^{-3}.

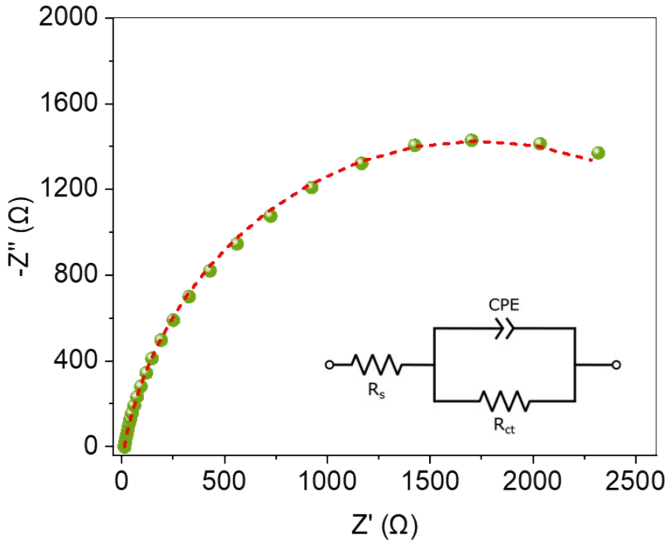

Fig. S18 Nyquist plot (Inset: equivalent circuit model used to fit the EIS data) of the β-Ni(OH)$_2$ microparticles. The red line is fit of the experimental data. The fitting analysis yielded a charge-transfer resistance (R_{ct}) of 3437 ohm.

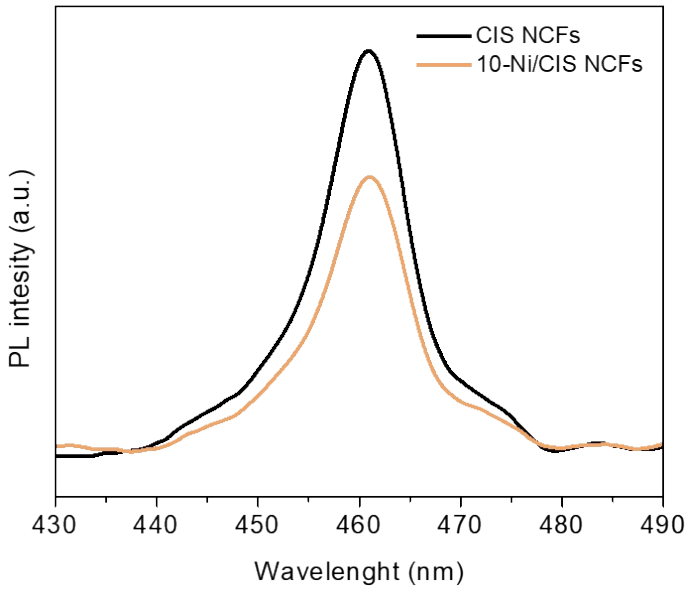

Fig. S19 Room temperature PL emission spectra of the mesoporous CIS and 10-Ni/CIS NCFs. PL experiments were carried out in water (1 mg mL^{-1}) under 375 nm excitation wavelength.

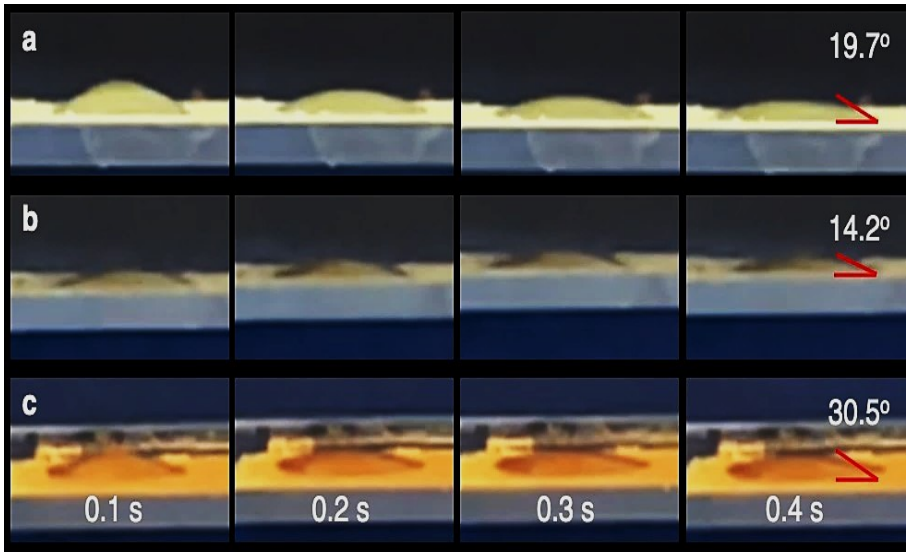

Fig. S20 Contact angle measurements of the mesoporous (a) CIS and (b) 10-Ni/CIS NCFs, and (c) bulk 10-Ni/CIS-*m*. The diameter of the water droplet was approximately 2 nm.

References

(1) C. Li, Y. Zhao, X. Liu, P. Huo, Y. Yan, L. Wang, G. Liao and C. Liu, *J. Colloid Interface Sci.*, 2021, **600**, 794–803.
(2) L. Peng, C. Yu, Y. Ma, G. Xie, X. Xie, Z. Wu and N. Zhang, *Inorg. Chem. Front.*, 2022, **9**, 994–1005.
(3) X. Li, X. Yan, N. Zhao, J. Zhao, B. Lu, X. Zhang, X. Zhang and H. Yu, *J. Photochem. Photobiol. A*, 2018, **360**, 298–305.
(4) Y. T. Prabhu, R. Kumari, A. Gautam, B. Sreedhar and U. Pal, *Nano-Structures & Nano-Objects*, 2021, **26**, 100682.
(5) R. Fu, Y. Gong, C. Li, L. Niu and X. Liu, *Nanomaterials*, 2021, **11**, 3122.
(6) C. Xue, H. An, X. Yan, J. Li, B. Yang, J. Wei and G. Yang, *Nano Energy*, 2017, **39**, 513–523.
(7) S. Guo, Y. Li, C. Xue, Y. Sun, C. Wu, G. Shao and P. Zhang, *Chem. Eng. J.*, 2021, **419**, 129213.
(8) L. Xie, G. Liu, R. Suo, Z. Xie, H. Liu, J. Chen, J. Chen and C.-Z. Lu, *J. Alloys Compd.*, 2023, **948**, 169692.
(9) X. Dang, M. Xie, F. Dai, J. Guo, J. Liu and X. Lu, *J. Mater. Chem. A*, 2021, **9**, 14888–14896.
(10) J. Xu, Q. Li, D. Sui, W. Jiang, F. Liu, X. Gu, Y. Zhao, P. Ying, L. Mao, X. Cai and J. Zhang, *Nanomaterials*, 2023, **13**, 420.
(11) W. Yang, S. S. Xu, Y. Niu, Y. Zhang and J. Xu, *J. Phys. Chem. C*, 2023, **127**, 4853–486.
(12) X. Li Li, X. J. Wang, J. Y. Zhu, Y. P. Li, J. Zhao and F. T. Li, *Chem. Eng. J.*, 2018, **353**, 15–24.
(13) Z. Xiang, H. Guan, B. Zhang and Y. Zhao, *J. Am. Ceram. Soc.*, 2021, **104**, 504–513.
(14) Z. Yang, L. Shao, L. Wang, X. Xia, Y. Liu, S. Cheng, C. Yang and S. Li, *Int. J. Hydrogen Energy*, 2020, **45**, 14334–14346.
(15) D. Zeng, Z. Lu, X. Gao, B. Wu and W. J. Ong, *Catal. Sci. Technol.*, 2019, **9**, 4010–4016.
(16) B. Wu, N. Liu, L. Lu, R. Zhang, R. Zhang, W. Shi and P. Cheng, *Chem. Commun.*, 2022, **58**, 6622–6625.
(17) E. K. Andreou, I. Vamvasakis and G. S. Armatas, *Adv. Mater. Interfaces*, 2024, **11**, 2300994.